An integral equation method for the inverse conductivity problem.

S. Ciulli[†], *M.K. Pidcock*[‡] *and C. Sebu*[†]

[†]*Laboratoire de Physique–Mathématique et Théorique, Université de Montpellier II, 34095 Montpellier, France;*

[‡]*Department of Mathematical Sciences, Oxford Brookes University, Oxford OX33 1HX, United Kingdom.*

PM 04-04

To be published in Physics Letters A

Abstract: *We present an image reconstruction algorithm for the Inverse Conductivity Problem based on reformulating the problem in terms of integral equations. We use as data the values of injected electric currents and of the corresponding induced boundary potentials, as well as the boundary values of the electrical conductivity.*

We have used a priori information to find a regularized conductivity distribution by first solving a Fredholm integral equation of the second kind for the Laplacian of the potential, and then by solving a first order partial differential equation for the regularized conductivity itself. Many of the calculations involved in the method can be achieved analytically using the eigenfunctions of an integral operator defined in the paper.

Keywords : Inverse conductivity Problem, Nonlinear inverse problems, Electrical Impedance Tomography, Land mine detection.

1. Introduction

It is well-known that the inverse conductivity problem is an extremely ill-posed, non-linear inverse problem, and there has been much interest in determining the class of conductivity distributions that can be recovered from the boundary data, as well as in the development of related reconstruction algorithms. The interest in this problem has been generated by both difficult theoretical challenges and by the important medical, geophysical and industrial applications of this problem. Much theoretical work has been related to the approach of Calderón concerning the bijection between the Neumann-to-Dirichlet operator, which relates the distribution of the injected currents to the boundary values of the induced electrical potential and the conductivity inside the region [1–4]. The reconstruction procedures that have been proposed include a wide range of iterative methods based on formulating the inverse problem as a nonlinear optimisation problem. These techniques are quite demanding computationally particularly when addressing the three dimensional problem. This concern has encouraged the search for reconstruction algorithms which reduce the computational demands either by using some *a priori* information e.g. [5–7] or by developing non iterative procedures. Some of these methods [6, 7] use a factorization approach while others are based on reformulating the inverse problems in terms of integral equations [8–10].

In [9] we presented one such approach which we applied to a two dimensional bounded domain while in [10] we extended this work to an unbounded three dimensional region. A feature of this method is the use of *a priori* information to find the regularized conductivity. This represents an additional requirement of our method but in some cases information on the internal structure of the object is already available. In return this enables us to make an estimate of the conductivity using a single data set. Another feature is that many of the calculations involve working with analytical expressions containing the eigenfunctions of the kernel of these equations, the computational part being restricted of the introduction of the data, the numerical evaluation of some of the analytic formulæ and the solution of a final integral equation. However, this first version of our method requires the knowledge on the boundary $\partial\Omega$ of the region Ω not only of the electrical potential Φ and its normal derivative $\partial\Phi/\partial n$, but also of the electrical conductivity σ and its normal derivative $\partial\sigma/\partial n$. In geophysics the conductivity

function at the surface can be measured by taking small soil samples, whilst in medical applications this might be achieved using closely spaced electrodes. Although in geophysics it is sometimes also possible to measure the derivative of the conductivity, in medical applications this is more difficult.

In this paper we describe a new version of our approach which no longer requires the knowledge of $\partial\sigma/\partial n$, but uses only data which is easily measurable on the boundary: namely the boundary values of the conductivity function σ, the injected currents (i.e. $\partial\Phi/\partial n|_{\partial\Omega}$) and the corresponding values of the induced potentials $\Phi|_{\partial\Omega}$. We will show that this information is sufficient to find a *regularised* solution $\sigma_{reg}(\mathbf{x})$ for the conductivity. This new approach differs from our previous work [9, 10] also in that the final step in the reconstruction algorithm involves the solution of a first order linear partial differential equation rather than one of second order.

Throughout this paper we shall assume that the conductivity distribution $\sigma \in C^1(\overline{\Omega})$. Such functions are dense in the larger class of the functions which have these properties only piecewise and which contains many of the physically interesting situations. In addition we shall assume that the domain Ω is a bounded open set whose boundary $\partial\Omega$ is sufficiently smooth, namely of class C^2.

Identification problems for elliptic equations have been the object of many studies in other fields as hydrology and diffusion equation [11–15].

2. Problem formulation

From the conservation of the current density $j(\mathbf{x})$ it follows that in the case of a general isotropic conductivity distribution $\sigma(\mathbf{x})$, the potential $\Phi(\mathbf{x})$ satisfies :

$$\nabla \cdot [\,\sigma(\mathbf{x})\nabla\Phi(\mathbf{x})\,] = 0\,, \qquad \mathbf{x} \in \Omega \subset \mathbb{R}^n\,, \quad n = 2\,, 3\,. \tag{1}$$

The inverse conductivity problem considered in this paper can be stated as follows: from the values of σ, Φ and $\partial\Phi/\partial n$ on the boundary $\partial\Omega$, reconstruct the conductivity function $\sigma(\mathbf{x})$ in Ω.

If we define $\widetilde{\sigma}(\mathbf{x}) \equiv ln(\sigma(\mathbf{x}))$, equation (1) can be rewritten as

$$\nabla^2\Phi(\mathbf{x}) = -Y(\mathbf{x})\,, \;\; \text{with} \;\; \mathrm{Y}(\mathbf{x}) \equiv \nabla\widetilde{\sigma}(\mathbf{x}) \cdot \nabla\Phi(\mathbf{x})\,. \tag{2}$$

This equation has the advantage that the (*not singular*) solution $\widetilde{\sigma}(\mathbf{x})$ to the inverse problem formulated in this way ensures the positivity of the conductivity $\sigma(\mathbf{x})$. To find $\widetilde{\sigma}(\mathbf{x})$ we will first reconstruct the potential $\Phi(\mathbf{x})$ everywhere in Ω from the information available on the boundary. We will then solve the differential equation for $\widetilde{\sigma}(\mathbf{x})$ using the method of characteristics. In this case, equation (2) reads

$$\frac{d\widetilde{\sigma}(\mathbf{x}(s))}{ds} = \frac{1}{|\nabla\Phi|} Y(\mathbf{x}(s))\,, \tag{3}$$

where s is the distance measured along the characteristics.

By using Green's formula, we can transform the partial differential equation (2) and the boundary information into an equivalent pair of integral equations

$$\Phi(\mathbf{x}) \;=\; \chi_D(\mathbf{x}) \,+\, \int\limits_{\Omega} d^n\mathbf{y}\, \mathcal{G}_D(\mathbf{x},\mathbf{y})\, Y(\mathbf{y}) \tag{4}$$

$$\Phi(\mathbf{x}) \;=\; \chi_N(\mathbf{x}) \,+\, \int\limits_{\Omega} d^n\mathbf{y}\, \mathcal{G}_N(\mathbf{x},\mathbf{y})\, Y(\mathbf{y})\,, \tag{5}$$

where $\mathcal{G}_D$ and $\mathcal{G}_N$ are the Dirichlet and Neumann Green's functions for Laplace's equation in Ω. Here χ_D and χ_N are the two harmonic functions constructed respectively from the measured Dirichlet and Neumann boundary data, $\Phi|_{\partial\Omega}$ and $\partial\Phi/\partial n|_{\partial\Omega}$:

$$\chi_D(\mathbf{x}) \;=\; -\int\limits_{\partial\Omega} d^{n-1}\mathbf{z}\, \frac{\partial\mathcal{G}_D}{\partial n}(\mathbf{x},\mathbf{z})\;\; \Phi(\mathbf{z})|_{\partial\Omega} \tag{6}$$

$$\chi_N(\mathbf{x}) \;=\; \int\limits_{\partial\Omega} d^{n-1}\mathbf{z}\, \mathcal{G}_N(\mathbf{x},\mathbf{z})\; \frac{\partial\Phi}{\partial n}\Big|_{\partial\Omega} + \frac{C}{\mid \partial\Omega \mid}\,. \tag{7}$$

where $C = \int\limits_{\partial\Omega} \Phi(\mathbf{z}) d^{n-1}\mathbf{z}$. These functions are different unless $\sigma(\mathbf{x})$ is a constant.

Theorem 1 *The knowledge of $\sigma(\mathbf{x})$ on $\partial\Omega$ and of $\Phi(\mathbf{x})$ in Ω uniquely determines $\sigma(\mathbf{x})$ in Ω.*

Proof Suppose that $\widetilde{\sigma}_1$ and $\widetilde{\sigma}_2$ are two functions satisfying equation (2) and $\widetilde{\sigma}_1 \neq \widetilde{\sigma}_2$. Define $\widetilde{\sigma}_{diff} = \widetilde{\sigma}_1 - \widetilde{\sigma}_2$. Then

$$\nabla^2\Phi(\mathbf{x}) = -\nabla\widetilde{\sigma}_1(\mathbf{x})\cdot\nabla\Phi(\mathbf{x}) = -\nabla\widetilde{\sigma}_2(\mathbf{x})\cdot\nabla\Phi(\mathbf{x})\,,\;\; \mathbf{x}\in\Omega \tag{8}$$

$$\nabla\widetilde{\sigma}_{diff}\cdot\nabla\Phi(\mathbf{x}) = 0\,,\;\; \mathbf{x}\in\Omega\,. \tag{9}$$

In other words, the function $\widetilde{\sigma}_{diff}(\mathbf{x})$ is constant along the current lines inside Ω. Since σ is known on $\partial\Omega$ we have $\widetilde{\sigma}_{diff}(\mathbf{x}) = 0\,,\;\; \mathbf{x}\in\partial\Omega$. Hence, provided that through any point $\mathbf{x}\in\Omega$ there passes a current line that intersects the boundary $\partial\Omega$ [see remark below and [12]], it follows that

$$\widetilde{\sigma}_{diff}(\mathbf{x}) = 0\,,\;\; \mathbf{x}\in\Omega\,. \tag{10}$$

Thus, $\widetilde{\sigma}$ is unique and it follows from the monotonicity of the logarithmic function that so too is σ. □

Remark It is important to verify that through each interior point of Ω passes a current line which continues up to the boundary. The danger with the current lines of a general vector field is that they may spin indefinitely without reaching the boundary, as happens with solenoidal fields. Since in our case the vector field is of gradient type, it is irrotational and so the field lines cannot terminate inside the domain [16] but must continue up to the boundary. Of course, there might be some singular points where, for example, the gradient vanishes but as is known from Morse Theory [17], as long we are interested only in *generic cases*, these singular points are isolated. There exist extreme situations (e.g. constant fields) for which the current lines avoid large regions, but any generic changes, even infinitesimal, will lead to one of these (*generic*) *Morse Fields* in which σ can be constructed from its boundary values everywhere, except at most at some isolated points where it can be found using continuity.

3. The Direct Problem

Before considering the Inverse Problem, let us see how one can compute the potential Φ if the conductivity σ is known. For instance, as shown in [9, 10], one may use the well known change of variable $\tau = \sqrt{\sigma}$ to transform equation (1) into an integral equation for the function $\Psi \equiv \tau\Phi$. Another way consists of applying the operator $\nabla_{\mathbf{x}}\widetilde{\sigma}(\mathbf{x})\cdot\nabla_{\mathbf{x}}$ to equation (4) to give

$$Y(\mathbf{x}) = \nabla_{\mathbf{x}}\widetilde{\sigma}(\mathbf{x})\cdot\nabla_{\mathbf{x}}\chi_D(\mathbf{x}) + \int\limits_{\Omega} d^n\mathbf{y}\, K(\mathbf{x},\mathbf{y})\, Y(\mathbf{y})\,, \tag{11}$$

where $K(\mathbf{x},\mathbf{y}) = \nabla_{\mathbf{x}}\widetilde{\sigma}(\mathbf{x})\cdot\nabla_{\mathbf{x}}\mathcal{G}_D(\mathbf{x},\mathbf{y})$. This is an integral equation for the Laplacian $Y(\mathbf{x})$ of $\Phi(\mathbf{x})$. Once $Y(\mathbf{x})$ is known, one can compute $\Phi(\mathbf{x})$ by means of a quadrature using the formula (4) or (5).

It would be nice for the practical solution of equation (11) if the integral operator defined by the kernel $K(\mathbf{x},\mathbf{y})$ were compact, since compact operators imply the Fredholm Alternative [18]. For that it is sufficient that $K\in L^2(\Omega^2)$, but $\int\limits_{\Omega} d^n\mathbf{x}\int\limits_{\Omega} d^n\mathbf{y}\;|\nabla_{\mathbf{x}}\widetilde{\sigma}(\mathbf{x})\cdot\nabla_{\mathbf{x}}\mathcal{G}_D(\mathbf{x},\mathbf{y})|^2$ is divergent because of the singularity of $\nabla_{\mathbf{x}}\mathcal{G}_D(\mathbf{x},\mathbf{y})$. However, we shall show that the situation can be recovered by considering the first iteration of equation (11) .

Theorem 2 *If $\sigma\in C^1(\Omega)$, the first iterated kernel of equation (11) $K_2(\mathbf{x},\mathbf{z}) = \int\limits_{\Omega} d^n\mathbf{y}\, K(\mathbf{x},\mathbf{y})K(\mathbf{y},\mathbf{z})$ is Hilbert-Schmidt.*

Proof We shall prove that the first iterated kernel

$$K_2(\mathbf{x},\mathbf{z}) \equiv \int\limits_{\Omega} d^3\mathbf{y}\, \nabla_{\mathbf{x}}\widetilde{\sigma}(\mathbf{x})\cdot\nabla_{\mathbf{x}}\mathcal{G}_D(\mathbf{x},\mathbf{y})\nabla_{\mathbf{y}}\widetilde{\sigma}(\mathbf{y})\cdot\nabla_{\mathbf{y}}\mathcal{G}_D(\mathbf{y},\mathbf{z}) \tag{12}$$

is Hilbert-Schmidt. For smooth conductivities σ in Ω, any singular behaviour in the integrand comes from the gradient of the Dirichlet Green's function. We consider here only the three dimensional case but the proof in two dimensions is similar. Although in two dimensions the first iterated kernel K_2 has a weak singularity (of logarithmic type) it is also Hilbert-Schmidt.

We study only the leading singularity which is of the form

$$\nabla_{\mathbf{x}}\mathcal{G}_D(\mathbf{x},\mathbf{y}) \sim \frac{1}{4\pi}\frac{\mathbf{x}-\mathbf{y}}{|\mathbf{x}-\mathbf{y}|^3}\,.$$

Since $\widetilde{\sigma}\in C^1(\Omega)$, for any $\epsilon>0$ there exists a ball $\Omega_R\subset\Omega$ of radius R with centre $\mathbf{x}\in\Omega$ such that

$$|\nabla_{\mathbf{x}}\widetilde{\sigma}(\mathbf{x})-\nabla_{\mathbf{y}}\widetilde{\sigma}(\mathbf{y})|<\epsilon\,,\quad \forall\mathbf{y}\in\Omega_R$$

Hence, in this ball we can approximate $\nabla_{\mathbf{y}}\widetilde{\sigma}(\mathbf{y})$ by $\nabla_{\mathbf{x}}\widetilde{\sigma}(\mathbf{x})$. The most singular parts of $K_2(\mathbf{x},\mathbf{z})$ can be written as

$$K_2(\mathbf{x},\mathbf{z}) \sim K_2^1(\mathbf{x},\mathbf{z}) + K_2^2(\mathbf{x},\mathbf{z}) \tag{13}$$

where

$$K_2^1(\mathbf{x},\mathbf{z}) = \frac{1}{16\pi^2}\int\limits_{\Omega\backslash\Omega_R} d^3\mathbf{y}\,\nabla_{\mathbf{x}}\widetilde{\sigma}(\mathbf{x})\cdot\frac{(\mathbf{x}-\mathbf{y})}{|\mathbf{x}-\mathbf{y}|^3}\nabla_{\mathbf{y}}\widetilde{\sigma}(\mathbf{y})\cdot\frac{(\mathbf{y}-\mathbf{z})}{|\mathbf{y}-\mathbf{z}|^3}$$

and

$$K_2^2(\mathbf{x},\mathbf{z}) = \frac{1}{16\pi^2}\int\limits_{\Omega_R} d^3\mathbf{y}\,\nabla_{\mathbf{x}}\widetilde{\sigma}(\mathbf{x})\cdot\frac{(\mathbf{x}-\mathbf{y})}{|\mathbf{x}-\mathbf{y}|^3}\nabla_{\mathbf{x}}\widetilde{\sigma}(\mathbf{x})\cdot\frac{(\mathbf{y}-\mathbf{z})}{|\mathbf{y}-\mathbf{z}|^3}\,.$$

Since the modulus of the gradient of $\widetilde{\sigma}$ is bounded on Ω, we have

$$\left|K_2^1(\mathbf{x},\mathbf{z})\right| < \frac{Const}{16\pi^2}\int\limits_{\Omega\backslash\Omega_R} d^3y\;\frac{1}{|\mathbf{x}-\mathbf{y}|^2}\frac{1}{|\mathbf{y}-\mathbf{z}|^2}\,.$$

When studying the limit $r=|\mathbf{x}-\mathbf{z}|\to 0$ we can take $r<R/N<<R$ for some $N\in\mathbb{N}$. Then, for $\mathbf{y}\in\Omega\backslash\Omega_R$, it follows that $|\mathbf{y}-\mathbf{x}|>R$ and $|\mathbf{y}-\mathbf{z}|>R(1-1/N)$, and hence

$$\left|K_2^1(\mathbf{x},\mathbf{z})\right| < \frac{Const}{16\pi^2}\frac{|\Omega|}{(1-1/N)^2R^4}\,. \tag{14}$$

To evaluate $K_2^2(\mathbf{x},\mathbf{z})$ we define $\mathbf{x}=(0,0,0)$, $\mathbf{z}=(0,0,r)$ and $\mathbf{y}=(\rho\sin\theta\cos\phi,\rho\sin\theta\sin\phi,\rho\cos\theta)$, where $(\rho,\theta,\phi)\in\mathbb{R}^3$ are local spherical coordinates in Ω_R. The constant gradient of $\widetilde{\sigma}$ points in an arbitrary direction, so for illustration we shall consider $\nabla_{\mathbf{x}}\widetilde{\sigma}(\mathbf{x})=(0,0,1)$. In this case

$$K_2^2(\mathbf{x},\mathbf{z}) \;\sim\; \frac{1}{8\pi}\int\limits_0^R d\rho\int\limits_0^\pi \sin\theta d\theta\frac{\cos\theta(\rho\cos\theta-r)}{(\rho^2-2\rho r\cos\theta+r^2)^{\frac{3}{2}}} \;=\; -\frac{1}{12\pi R}\,. \tag{15}$$

Combining equations (14) and (15) we see that $K_2(\mathbf{x},\mathbf{z})$ remains finite as $|\mathbf{x}-\mathbf{z}|\equiv r\to 0$ and hence is Hilbert-Schmidt. □

This theorem implies that the first iteration of equation (11), namely

$$Y(\mathbf{x}) = \nabla_{\mathbf{x}}\widetilde{\sigma}(\mathbf{x})\cdot\nabla_{\mathbf{x}}\chi_D(\mathbf{x}) + \int\limits_{\Omega} d^n\mathbf{y}\,K(\mathbf{x},\mathbf{y})\nabla_{\mathbf{y}}\widetilde{\sigma}(\mathbf{y})\cdot\nabla_{\mathbf{y}}\chi_D(\mathbf{y}) + \int\limits_{\Omega} d^n\mathbf{y}\,K_2(\mathbf{x},\mathbf{y}))\,Y(\mathbf{y}) \tag{16}$$

can be solved by means of the usual numerical procedures for Fredholm equations. Once the function $Y(\mathbf{x})$ has been computed, the potential $\Phi(\mathbf{x})$ can be obtained by means of the formulæ (4) or (5). This procedure can then be used to perform simulations to study the performance of our method of solving the Inverse Problem.

4. The Unregularized Inverse Problem

Initially, our treatment of the inverse problem is similar to that described in [9,10]. Subtracting equation (4) from (5) we have

$$\chi(\mathbf{x}) - \int_{\Omega} d^n\mathbf{y}\, \mathcal{K}(\mathbf{x},\mathbf{y})\, Y(\mathbf{y}) = 0 \tag{17}$$

where

$$\mathcal{K}(\mathbf{x},\mathbf{y}) = \mathcal{G}_D(\mathbf{x},\mathbf{y}) - \mathcal{G}_N(\mathbf{x},\mathbf{y}) \quad \text{and} \quad \chi(\mathbf{x}) = \chi_{\mathrm{N}}(\mathbf{x}) - \chi_{\mathrm{D}}(\mathbf{x})\,.$$

Equation(17) is an ill-posed Fredholm integral equation of the first kind. Since the kernel $\mathcal{K}(\mathbf{x},\mathbf{y})$ is the difference of two Green's functions it is harmonic and symmetric. The null space $N(\mathcal{K})$ of $\mathcal{K}$ consists of all the functions which are orthogonal to the harmonic functions in Ω. We can prove the following result concerning the potentials $\Phi_{\mathfrak{k}}$ related to this null space.

Theorem 3 *Within the set of functions* $\{\Phi_{\mathfrak{k}}\}$ *that satisfy* $\nabla^2\Phi_{\mathfrak{k}} = -Y_{\mathfrak{k}}$ *where* $Y_{\mathfrak{k}} \in N(\mathcal{K})$ *there exists at least one function such that* $\Phi_{\mathfrak{k}}(\mathbf{x})|_{\partial\Omega} = 0$ *and* $\frac{\partial\Phi_{\mathfrak{k}}}{\partial n}(\mathbf{x})\Big|_{\partial\Omega} = 0$.

Note: Such a function is, of course, completely invisible to any measurement of potentials and currents on the boundary.

Proof Since the Laplacian of any harmonic function is identically zero, it is clear that the functions $\Phi_{\mathfrak{k}}$ are defined only up to an harmonic function Φ_h. So, if the boundary values of some initial $\Phi'_{\mathfrak{k}}$ are not zero, we can always find another function $\Phi_{\mathfrak{k}} = \Phi'_{\mathfrak{k}} + \Phi_h$, having the same Laplacian $(-Y_{\mathfrak{k}})$, but with

$$\Phi_{\mathfrak{k}}|_{\partial\Omega} = 0\,. \tag{18}$$

To this end it is sufficient to take

$$\Phi_h(\mathbf{x}) = \int_{\partial\Omega} d^{n-1}\mathbf{y} \frac{\partial\mathcal{G}_D(\mathbf{x},\mathbf{y})}{\partial n}\Phi'_{\mathfrak{k}}(\mathbf{y})\,, \tag{19}$$

where the function Φ_h is harmonic and has by construction boundary values which are opposite to that of $\Phi'_{\mathfrak{k}}$. So $\Phi_{\mathfrak{k}}|_{\partial\Omega} = 0$.

To prove that the normal derivative of $\Phi_{\mathfrak{k}}$ is identically zero on the boundary, we use Green's formula

$$\int_{\Omega} d^n\mathbf{x}\, \left(u(\mathbf{x})\,\nabla^2\Phi_{\mathfrak{k}}(\mathbf{x}) \,-\, \Phi_{\mathfrak{k}}(\mathbf{x})\nabla^2 u(\mathbf{x})\right) \,=\, \int_{\partial\Omega} d^{n-1}\mathbf{x}\, \left(u(\mathbf{x})\,\frac{\partial\Phi_{\mathfrak{k}}(\mathbf{x})}{\partial n} \,-\, \Phi_{\mathfrak{k}}(\mathbf{x})\,\frac{\partial u(\mathbf{x})}{\partial n}\right)\,, \tag{20}$$

where $u(\mathbf{x})$ is any harmonic function in Ω. Since $\nabla^2 u = 0$ and since $\nabla^2\Phi_{\mathfrak{k}} = -Y_{\mathfrak{k}}$ is orthogonal to any harmonic function, the left hand side of the above equation is zero. But from (18) $\Phi_{\mathfrak{k}}|_{\partial\Omega} \equiv 0$, we see that

$$\int_{\partial\Omega} d^{n-1}\mathbf{x}\, u(\mathbf{x})\,\frac{\partial\Phi_{\mathfrak{k}}(\mathbf{x})}{\partial n} \,=\, 0\,. \tag{21}$$

Let us assume for a moment that at some given point $x_0 \in \partial\Omega$ the normal derivative were not zero, $\partial\Phi_{\mathfrak{k}}(\mathbf{x})/\partial n|_{\mathbf{x}=\mathbf{x_0}} \neq 0$. Since according to our general assumptions the derivatives of Φ are continuous in $\overline{\Omega}$ — i.e. also on $\partial\Omega$ — there exists a neighbourhood on the boundary $\partial\Omega_{\epsilon,x_0} \subset \partial\Omega$ of $x_0 \in \partial\Omega$,

on which this derivative has the same sign. Considering for $u(\mathbf{x})$ the harmonic measure defined by the boundary conditions

$$u(\mathbf{x})|_{\mathbf{x}\in\partial\Omega} \;=\; \begin{cases} 1 \;\;, & if\ \mathbf{x}\in\partial\Omega_{\epsilon,x_0}\,, \\ 0 \;\;, & elsewhere\ on\ \partial\Omega. \end{cases} \tag{22}$$

we see that if $\partial\Phi_{\mathfrak{k}}/\partial n$ were not identically zero on $\partial\Omega$, the integral (21) cannot be zero. As a consequence both $\Phi_{\mathfrak{k}}(\mathbf{x})$ and $\partial\Phi_{\mathfrak{k}}(\mathbf{x})/\partial n$ have to vanish identically on $\partial\Omega$. □

An example of such a function can be constructed explicitly from the function $Y_{\mathfrak{k}}$, as described in the following Lemma.

Lemma 1 *The function* $\Phi_{\mathfrak{k}}(\mathbf{x}) = \int\limits_{\Omega} d^n\mathbf{y}\,\mathcal{G}_D(\mathbf{x},\mathbf{y})Y_{\mathfrak{k}}(\mathbf{y})$*, where* $Y_{\mathfrak{k}}\in N(\mathcal{K})$*, has the properties stated in Theorem 3 i.e.: (i)* $\nabla^2\Phi_{\mathfrak{k}} = -Y_{\mathfrak{k}}\ \ \mathbf{x}\in\Omega$*, (ii)* $\Phi_{\mathfrak{k}}(\mathbf{x}) = 0\,,\ \ \mathbf{x}\in\partial\Omega$*, (iii)* $\frac{\partial\Phi_{\mathfrak{k}}}{\partial n}(\mathbf{x}) = 0\,,\ \ \mathbf{x}\in\partial\Omega\,.$

Proof (i) If $x\in\Omega$, then

$$\nabla^2\Phi_{\mathfrak{k}}(\mathbf{x}) = \int\limits_{\Omega} d^n\mathbf{y}\,\nabla^2\mathcal{G}_D(\mathbf{x},\mathbf{y})Y_{\mathfrak{k}}(\mathbf{y}) = -\int\limits_{\Omega} d^n\mathbf{y}\delta(\mathbf{x}-\mathbf{y})Y_{\mathfrak{k}}(\mathbf{y}) = -Y_{\mathfrak{k}}(\mathbf{y})\,.$$

(*ii*) If $\mathbf{x}\in\partial\Omega$, recall that $\mathcal{G}_D(\mathbf{x},\mathbf{y}) = 0$ and hence $\Phi_{\mathfrak{k}}(\mathbf{x}) = \int\limits_{\Omega} d^n\mathbf{y}\,\mathcal{G}_D(\mathbf{x},\mathbf{y})Y_{\mathfrak{k}}(\mathbf{y}) = 0\,.$

(*iii*) If $Y_{\mathfrak{k}}\in N(\mathcal{K})$ and $\mathcal{K}(\mathbf{x},\mathbf{y}) = \mathcal{G}_D(\mathbf{x},\mathbf{y}) - \mathcal{G}_N(\mathbf{x},\mathbf{y})$ it follows that

$$\Phi_{\mathfrak{k}}(\mathbf{x}) = \int\limits_{\Omega} d^n\mathbf{y}\,\mathcal{G}_N(\mathbf{x},\mathbf{y})Y_{\mathfrak{k}}(\mathbf{y})\,,\ \ \mathbf{x}\in\Omega$$

is also a valid representation for $\Phi_{\mathfrak{k}}$. Moreover, $\left.\frac{\partial\mathcal{G}_N(\mathbf{x},\mathbf{y})}{\partial n}\right|_{\mathbf{x}\in\partial\Omega} = -\frac{1}{|\partial\Omega|}$, so that

$$\left.\frac{\partial\Phi_{\mathfrak{k}}}{\partial n}(\mathbf{x})\right|_{\mathbf{x}\in\partial\Omega} = -\frac{1}{|\partial\Omega|}\int\limits_{\Omega} d^n\mathbf{y}\,Y_{\mathfrak{k}}(\mathbf{y}) = 0$$

since $Y_{\mathfrak{k}}(\mathbf{y})$ is orthogonal to any harmonic function in Ω and the constant 1 is an harmonic function. □

Explicit analytical expressions of such functions $Y_{\mathfrak{k}}\in N(\mathcal{K})$ and their respective $\Phi_{\mathfrak{k}}$ for the unit disk are given in Section 6.

At this stage an apparent paradox may emerge. Consider the case $\Phi\equiv\Phi_{\mathfrak{k}}$ corresponding to $Y_{\mathfrak{k}}\in N(\mathcal{K})$. Since $\nabla\Phi_{\mathfrak{k}}$ is in general not identically zero throughout Ω (see, for example, the explicit expressions given in Section 6), one may be tempted to reconstruct $\widetilde{\sigma}$ inside Ω by solving along the characteristics the differential equation (3) using the given boundary data $\widetilde{\sigma}(\mathbf{x}) = \ln(\sigma(\mathbf{x}))$ for $\mathbf{x}\in\partial\Omega$. However,

$$\int\limits_{\Omega} d^n\mathbf{x}\,\sigma(\mathbf{x})\ |\ \nabla\Phi(\mathbf{x})\ |^2 = \int\limits_{\partial\Omega} d^{n-1}\mathbf{x}\,\sigma(\mathbf{x})\,\Phi_{\mathfrak{k}}(\mathbf{x})\,\frac{\partial\Phi_{\mathfrak{k}}(\mathbf{x})}{\partial n}\ = 0\,, \tag{23}$$

since both $\Phi_{\mathfrak{k}}(\mathbf{x})|_{\partial\Omega}$ and $\left.\frac{\partial\Phi_{\mathfrak{k}}}{\partial n}(\mathbf{x})\right|_{\partial\Omega}$ are identically zero. From the non-negativity of $\sigma(\mathbf{x}) = \exp(\widetilde{\sigma}(\mathbf{x}))$, the left hand side is positively defined and so σ has to be zero everywhere where $\nabla\Phi_{\mathfrak{k}}$ is not. The key of this apparent dilema is that equation (3) cannot be solved since the normal component of $\nabla\Phi_{\mathfrak{k}}$ vanishes when $\mathbf{x}$ approaches the boundary. This represents a barrier that cannot be overpassed ($\left|\frac{d\widetilde{\sigma}}{ds}\right|\to\infty$) by the information conveyed by the equation (3). On the other hand, if σ is constant, from equation (2) it follows that $Y_{\mathfrak{k}}$ has to vanish identically throughout Ω, i.e. the coefficients $A_{k,n}$ and $B_{k,n}$ in expression (33) have to be zero.

5. The Regularized Integral Equation

Equation (17) is a Fredholm equation of the first kind which is notoriously ill-posed and whose solution is extremely unstable with respect to the data measured on the boundary $\partial\Omega$. We shall stabilize it by using Tikhonov regularization and a model function $Y_{mod}(\mathbf{x})$ as a first estimate of the solution (see Figure 1). This function can be obtained starting with a model conductivity σ_{mod} and solving equation (11), or better its first iterate (16), to find $Y_{mod}(\mathbf{x})$. The function σ_{mod} can be obtained in a variety of ways including the use of prior knowledge from other imaging modalities, previous results in time evolving situations or using simple reconstruction estimates using fast algorithms. One example of the latter is a Factorization method described in [6,7]. In this method a large number of current patterns are applied to the object and using this data a simple test at each point within Ω is used to determine a piecewise constant internal structure. This algorithm gives good results in many circumstances although practical numerical difficulties introduce instability. Nevertheless, we can use a continuous approximation to these results as a suitable σ_{mod}.

The use of the regularizing function Y_{mod} leads to a Fredholm equation of the second kind which can be solved explicitly and which is stable with respect to the errors in the input data. Moreover the null space of $\mathcal{K}$ plays no particular role in the solution of Fredholm equation of the second kind which is unique unless the Lagrange multiplier defined below happens to be an eigenvalue of $\mathcal{K}$.

Indeed, the input data and hence the function $\chi(\mathbf{x})$ always contain some errors. Consequently we no longer require that equation (17) should be satisfied exactly, but we ask instead that the L^2 norm of the left hand side of (17) should be small while the solution Y_{reg} should be close to a model function Y_{mod}. Hence our problem reduces to finding

$$\epsilon_0 = min \, \| \chi(\mathbf{x}) \, - \, \mathbf{K}[Y_{reg}](\mathbf{x}) \, \|_{L^2} \, , \;\; \text{subject to} \;\; \| Y_{reg}(\mathbf{x}) \, - \, Y_{mod}(\mathbf{x}) \|_{L^2} \leq \delta \, . \tag{24}$$

Here $\mathbf{K}[Y_{reg}](\mathbf{x}) \equiv \int d^n\mathbf{y} \, \mathcal{K}(\mathbf{x},\mathbf{y}) \, Y_{reg}(\mathbf{y})$. In practical terms this means that instead of eq.(17) we consider the Lagrange multiplier formulation of Tikhonov regularization [19, 20], namely we seek the unrestricted minimum of the functional

$$\| \chi(\mathbf{x}) \, - \mathbf{K}[Y_{reg}](\mathbf{x}) \|^2_{L^2} \, + \, \mu \, \left(\| Y_{reg}(\mathbf{x}) \, - \, Y_{mod}(\mathbf{x}) \|^2_{L^2} \, - \, \delta^2 \right) \, ,$$

where μ is a Lagrange multiplier.

In many cases of practical interest the target function depends also on a small number of parameters α, for instance connected with the translation and/or rotation Euclidean group. Consequently we could include these parameters in the model function $Y_{mod}(\mathbf{x};\alpha)$ and seek the minimum $\epsilon_{0,min} \equiv \epsilon_0(\alpha_0)$ with respect to these parameters. Such an example is discussed in Section 8. Here ϵ_0 which is a functional of the data, or its minimum $\epsilon_{0,min}$ with respect to the possible parameters α, measures the degree [20] to which the initial integral equation (17) is satisfied. In other words, it reflects the accuracy of the experimental data by means of which (see eq.(7)) the input function $\chi(\mathbf{x})$ has been constructed.

The minimisation process yields the following regularized integral equation:

$$Y_{reg}(\mathbf{x}) \, = \, Y_{mod}(\mathbf{x}) \, + \, \lambda \int\limits_{\Omega} d^n\mathbf{y} \, \mathcal{K}(\mathbf{x},\mathbf{y}) \, \chi(\mathbf{y}) \, - \, \lambda \int\limits_{\Omega} d^n\mathbf{y} \, \mathcal{K}_2(\mathbf{x},\mathbf{y}) \, Y_{reg}(\mathbf{y}) \tag{25}$$

where $\mathcal{K}_2(\mathbf{x},\mathbf{y}) \, \equiv \, \int\limits_{\Omega} d^n\mathbf{z} \, \mathcal{K}(\mathbf{x},\mathbf{z}) \, \mathcal{K}(\mathbf{z},\mathbf{y})$ and $\lambda \equiv 1/\mu$.

The eigenfunctions $\{u_k\}$ and eigenvalues $\{\lambda_k\}$ of $\mathcal{K}(\mathbf{x},\mathbf{y})$ satisfy $u_k(\mathbf{x}) = \lambda_k \int\limits_{\Omega} d^n\mathbf{y} \, \mathcal{K}(\mathbf{x},\mathbf{y}) \, u_k(\mathbf{y})$. If the kernel $\mathcal{K}(\mathbf{x},\mathbf{y})$ can be expressed in the form

$$\mathcal{K}(\mathbf{x},\mathbf{y}) \, = \, \sum_{k=1}^{\infty} \frac{u_k(\mathbf{x}) \, u_k(\mathbf{y})}{\lambda_k} \, ,$$

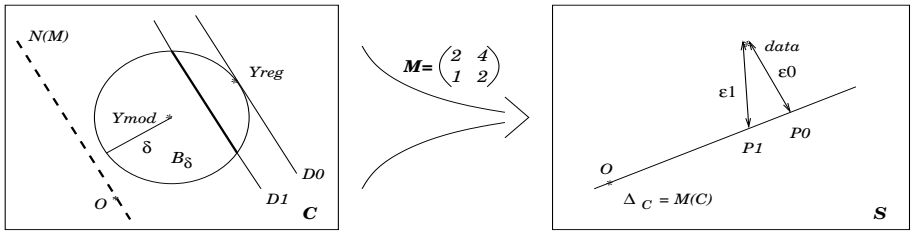

Figure 1:
For the Tikhonov regularisation it is not necessary that the mapping $\mathcal{M}$ between the *parameter* space $\mathcal{C}$ and the *data* space $\mathcal{S}$ should have a true inverse. The existence of a generalized inverse $\widehat{\mathcal{M}^{-1}}$ is sufficient. In the above figure the mapping transforming the $\mathcal{C}$ plane into the straight line $\Delta_C \in \mathcal{S}$ is provided by the non-invertible matrix $\begin{pmatrix} 2 & 4 \\ 1 & 2 \end{pmatrix}$ while the generalized inverse $\widehat{\mathcal{M}^{-1}}$ transforms the points $P_1,\ P_0 \in \Delta_C$ into the lines $D_1,\ D_0 \in \mathcal{C}$.
These low dimensional graphs may be misleading, as in infinite dimensions it might happen that there does not exist a smallest distance ϵ_0 between the *admissible* set $\Delta_C = \mathcal{M}(\mathcal{C})$ and the *data* $\notin \Delta_C$. Therefore, in infinite dimensional problems it is preferable to consider images of balls $\mathcal{B}$ from $\mathcal{C}$ rather than $\mathcal{M}(\mathcal{C})$ itself. Since in most physical problems the theorem of Banach-Alaoglu [22,23] also applies [24] , the images $\mathcal{M}(\mathcal{B})$ are true compact sets and the minimal distance ϵ_0 of such a set to the *data* is well defined. Nevertheless, the main features of these problems are well depicted by these figures, where the interesting points on the straight lines $D_1 ..., D_0$ are their intersections with the ball $\mathcal{B}_\delta$ of radius δ around Y_{mod}. Consequently, in our case the solution of the extremal problem will be the point $Y_{reg} \in D_0$.

we have a straightforward way to compute the eigenfunctions and eigenvalues and we can expand the iterated kernel $\mathcal{K}_2$ as:

$$\mathcal{K}_2(\mathbf{x},\mathbf{y}) \;=\; \sum_{k=1}^{\infty} \frac{u_k(\mathbf{x})\, u_k(\mathbf{y})}{\lambda_k^2}\,.$$

This is illustrated in the two dimensional example discussed in Section 6 (see also [21]).
Projecting Eq.(25) onto u_k we obtain

$$Y_{reg,k} \;=\; Y_{mod,k} \;+\; \frac{\lambda}{\lambda_k}\,\chi_k \;-\; \frac{\lambda}{\lambda_k^2}\,Y_{reg,k}$$

where

$$Y_{reg,k} = \int_\Omega d^n\mathbf{x}\, Y_{reg}(\mathbf{x}) u_k(\mathbf{x})\ ,\ Y_{mod,k} = \int_\Omega d^n\mathbf{x}\, Y_{mod}(\mathbf{x}) u_k(\mathbf{x})\ ,\ \chi_k = \int_\Omega d^n\mathbf{x}\, \chi(\mathbf{x}) u_k(\mathbf{x})\,,$$

and hence the following explicit expression for the solution $Y_{reg}(\mathbf{x})$:

$$Y_{reg}(\mathbf{x}) \;=\; Y_{mod}(\mathbf{x}) \;+\; \lambda \int_\Omega d\mathbf{y}^n\, \mathcal{K}(\mathbf{x},\mathbf{y})\, \chi(\mathbf{y}) \;-\; \lambda \sum_{k=1}^{\infty} \frac{Y_{mod,k} \;+\; \dfrac{\lambda}{\lambda_k}\,\chi_k}{\lambda \;+\; \lambda_k^2}\, u_k(\mathbf{x})\,. \tag{26}$$

Once $Y_{reg}(\mathbf{x})$ is known, the potential $\Phi_{reg}(\mathbf{x})$ can be obtained by means of the integral

$$\Phi_{reg}(\mathbf{x}) \;=\; \chi_D(\mathbf{x}) \;+\; \int_\Omega d^n\mathbf{y}\, \mathcal{G}_D(\mathbf{x},\mathbf{y})\, Y_{reg}(\mathbf{y})\,. \tag{27}$$

Finally, to determine the regularized $\sigma_{reg}(\mathbf{x})$, we can use the method of characteristics to solve the first order partial differential equation:

$$\nabla\widetilde{\sigma}_{reg}(\mathbf{x}) \cdot \nabla\Phi_{reg}(\mathbf{x}) - Y_{reg}(\mathbf{x}) = 0\,,\ \ \mathbf{x} \in \Omega \tag{28}$$

subject to the known boundary values $\widetilde{\sigma}(\mathbf{x})|_{\mathbf{x}\in\partial\Omega}$.

6. A two dimensional example: the unit disk

In this case the relevant Green's functions are:

$$\mathcal{G}_D(r,\theta;\rho,\vartheta) \;=\; -\frac{1}{4\pi}\,\log\frac{r^2+\rho^2-2r\rho\cos\left(\theta-\vartheta\right)}{1+r^2\rho^2-2r\rho\cos\left(\theta-\vartheta\right)} \tag{29}$$

$$\mathcal{G}_N(r,\theta;\rho,\vartheta) \;=\; -\frac{1}{4\pi}\,\log\left(\left(r^2+\rho^2-2r\rho\cos\left(\theta-\vartheta\right)\right)\cdot\left(1+r^2\rho^2-2r\rho\cos\left(\theta-\vartheta\right)\right)\right) \tag{30}$$

so that

$$\mathcal{K}(r,\theta;\rho,\vartheta) = \frac{1}{2\pi}\,\log\left(1+r^2\rho^2-2r\rho\cos\left(\theta-\vartheta\right)\right) \;-\; \sum_{k=1}^{\infty}\frac{r^k\rho^k\cos(k(\theta-\vartheta))}{\pi k}\,. \tag{31}$$

As remarked in Section 5, this series expansion enables us to find the eigenfunctions and eigenvalues of $\mathcal{K}$. Indeed, the functions $u_k^1(r,\theta)=\sqrt{(2k+2)/\pi}\;r^k\cos\,k\theta$ and $u_k^2(r,\theta)=\sqrt{(2k+2)/\pi}\;r^k\sin\,k\theta$ are orthonormal on the unit disk, so that $\mathcal{K}$ can be rewritten as

$$\mathcal{K}(r,\theta;\rho,\vartheta) \;=\; \sum_{k=1}^{\infty}\sum_{j=1}^{2}\frac{u_k^j\left(r,\theta\right)u_k^j\left(\rho,\vartheta\right)}{\lambda_k}\,,$$

with $\lambda_k=-2k(k+1)$.

From expansion (26) we obtain the following explicit expression for the solution of the regularized equation

$$Y_{reg}(r,\theta) \;=\; Y_{mod}(r,\theta)+\lambda\int_0^1\rho d\rho\int_0^{2\pi}d\vartheta\,\mathcal{K}(r,\theta;\rho,\vartheta)\,\chi(\rho,\vartheta)-\lambda\sum_{k=1}^{\infty}\sum_{j=1}^{2}\frac{Y_{mod,k}^j\;-\;\dfrac{\lambda}{2k(k+1)}\,\chi_k^j}{\lambda\;+\;4k^2(k+1)^2}\,u_k^j(r,\theta). \tag{32}$$

To find σ_{reg} we proceed in the way discussed at the end of Section 5.

Lemma 2 *For the unit disk the functions $Y_{\mathfrak{k}}\in N(\mathcal{K})$ have the explicit form*

$$Y_{\mathfrak{k}}(r,\theta)=\sum_{k=1}^{\infty}\sum_{n=1}^{\infty}G_n(k+2,k+2,r)\Big(A_{k,n}\cos(k\theta)+B_{k,n}\sin(k\theta)\Big)\,, \tag{33}$$

where $A_{k,n}$ and $B_{k,n}$ are arbitrary constants.

Proof If $Y_{\mathfrak{k}}\in N(\mathcal{K})$, then

$$\int_0^1\rho d\rho\int_0^{2\pi}d\vartheta\mathcal{K}(r,\theta;\rho,\vartheta)Y_{\mathfrak{k}}(\rho,\vartheta)=\sum_{k=1}^{\infty}\sum_{j=1}^{2}\frac{u_k^j\left(r,\theta\right)}{\lambda_k}\int_0^1\rho d\rho\int_0^{2\pi}d\vartheta\,u_k^j(\rho,\vartheta)Y_{\mathfrak{k}}(\rho,\vartheta)=0\,.$$

We start with a function $Y_{\mathfrak{k}}$ of the form

$$Y_{\mathfrak{k}}(r,\theta)=\Re_k(r)\cos(k\theta)\,,\quad k=1,2,3,\ldots\,.$$

which, in order to be in $N(\mathcal{K})$ must satisfy

$$\int_0^1\rho d\rho\int_0^{2\pi}d\vartheta u_k^1(r,\theta;\rho,\vartheta)Y_{\mathfrak{k}}(\rho,\vartheta)=-\sqrt{(2k+2)\pi}\int_0^1 d\rho\;\rho^{k+1}\Re_k(\rho)=0\,.$$

For this it is sufficient that

$$\Re_k(r,n) = G_n(k+2,k+2,r)\,, \text{for } n \geq 1\,,$$

where $G_n(k+2,k+2,r)$ are the Jacobi polynomials of order n [18].
If we consider

$$Y_{\mathfrak{k}}(r,\theta) = \Re_k(r)\sin(k\theta)\,,\ \ k = 1,2,3,\ldots\,.$$

we find a similar result. Our theorem follows by taking linear combinations of these results. □
Example: If we consider $Y_{\mathfrak{k}}(r,\theta) = G_1(3,3,r)\cos(\theta) = \left(1-\frac{4}{3}r\right)\cos(\theta) \in N(\mathcal{K})$ we can compute directly

$$\Phi_{\mathfrak{k}}(r,\theta) = \int_0^1 \rho d\rho \int_0^{2\pi} d\vartheta \mathcal{G}_D(r,\theta;\rho,\vartheta) Y_{\mathfrak{k}}(\rho\vartheta) = \frac{1}{6}r(r-1)^2\cos(\theta)\,.$$

7. A numerical example

We present here a numerical example to illustrate the performance of our algorithm. In this example we attempt to reconstruct a conductivity distribution consisting of two low conductivity regions and a high conductivity region within an uniform background. We represent this distribution mathematically by a function of the form:

$$\begin{aligned}\sigma_{exact}(x,y) &= 1 - 0.5\exp(-a((x-0.5)^2+(y-0.2)^2)^2) + \exp(-b((x+0.1)^2+(y-0.3)^2)^2) \\ &- 0.5\exp(-a((x+0.5)^2+(y+0.2)^2)^2)\,,\ \ x^2+y^2 \leq 1\,, \end{aligned} \tag{34}$$

which has a maximum at $(x,y) = (-0.1,0.3)$ and two minima at$(x,y) = (-0.5,-0.2)$ and $(x,y) = (0.5,0.2)$ (see Figure 2(a)). We chose $a = 1000$ and $b = 1500$.
We shall consider the input currents

$$\sigma(1,\theta)\frac{\partial\Phi}{\partial n}\bigg|_{\partial\Omega}(\theta) = \sin(m\theta)\,,\ \ m = 1,2,\ldots\,.$$

To simulate the measured values of the potential on the boundary we have to solve first the direct problem. The detailed numerical simulations can be found in [25]. With these data we can compute then the input function χ of our integral equation

$$\chi(r,\theta) = \int_0^{2\pi} d\vartheta \left\{ \mathcal{G}_N(r,\theta;1,\vartheta)\ \frac{\partial\Phi}{\partial n}\bigg|_{\partial\Omega}(\vartheta) + \left[\frac{1}{2\pi} + \frac{\partial\mathcal{G}_D}{\partial n}(r,\theta;1,\vartheta)\right]\Phi(1,\vartheta)\right\}\,.$$

To calculate the regularized solution Y_{reg} we need a model function Y_{mod}. To achieve this we need a model function for the conductivity σ_{mod}, which is in fact our *a priori* information. For the model function σ_{mod} we have used a conductivity distribution in which

- the positions of the low conductivity regions are quite well known but the size of these regions is more uncertain

- the size of the high conductivity region is quite well known but the position of this region is uncertain.

We have represented this model function mathematically as:

$$\begin{aligned}\sigma_{mod}(x,y) &= 1 - 0.7\exp(-a((x-0.6)^2+(y-0.3)^2)^3) + 1.2\exp(-b((x+0.4)^2+(y-0.7)^2)^2) \\ &- 0.7\exp(-a((x+0.6)^2+(y+0.3)^2)^3)\,, \end{aligned} \tag{35}$$

which lies at a distance $d \equiv \|\sigma_{mod} - \sigma_{exact}\|_{L^2} = 0.29\|\sigma_{exact}\|_{L^2}$ from the true function (see Figure 2(b)). This type of function could be a smooth approximation to piecewise constant approximates produced by [6, 7] as discussed in Section 5. By solving the forward problem as described in Section 3, we find

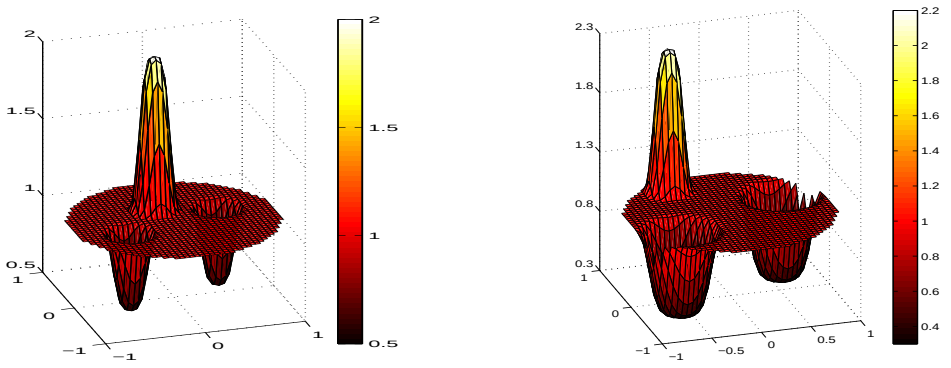

(a) (b)

Figure 2: (a) The exact conductivity σ_{exact}; (b) The model conductivity σ_{mod}.

the model potential Φ_{mod} and hence the model functions $Y_{mod}(x,y) = \nabla\widetilde{\sigma}_{mod}(x,y)\cdot\nabla\Phi_{mod}(x,y)$. By solving the forward problem as described in Section 3, we find the model potential Φ_{mod} and hence the model functions $Y_{mod}(x,y) = \nabla\widetilde{\sigma}_{mod}(x,y)\cdot\nabla\Phi_{mod}(x,y)$. The integral which appears in (32) can be computed numerically:

$$\int_0^1 \rho d\rho \int_0^{2\pi} d\vartheta \mathcal{K}(r,\theta;\rho,\vartheta)\chi(\rho,\vartheta) = \sum_{l=1}^{172} w_l \mathcal{K}(r,\theta;r_l,\theta_l)\chi(r_l,\theta_l)\,,$$

where $\{w_l; r_l, \theta_l\}$ is a set of quadrature weights and points for the unit disk [26]. Since, the infinite series which appear in equation (32) converges rapidly it was sufficient to consider only fifty terms to reach a precision of 10^{-8}.

There are many ways of determining the value of the parameter λ [19,27] and we have used the constraint (24) for a given value of δ. Once Y_{reg} is known, the calculation of the potential Φ inside the unit disk is straightforward:

$$\Phi(r,\theta) = \chi_D(r,\theta) + \sum_{l=1}^{172} w_l \mathcal{G}_D(r,\theta;r_l,\theta_l) Y_{reg}(r_l,\theta_l)\,,$$

where

$$\chi_D(r,\theta) = \frac{1-r^2}{2\pi}\int_0^{2\pi} \frac{\Phi(1,\vartheta)}{1+r^2-2r\cos(\theta-\vartheta)} d\vartheta\,.$$

The final step is to solve our first order partial differential equation (28). The method of characteristics transforms this equation into an equivalent system of ordinary differential equations which can be written in cartesian coordinates as:

$$\frac{dx}{ds} = \frac{d\Phi}{dx}(x(s),y(s))\,,\quad \frac{dy}{ds} = \frac{d\Phi}{dy}(x(s),y(s))\,,\quad \frac{d\widetilde{\sigma}}{ds} = Y_{reg}(x(s),y(s))\,. \tag{36}$$

We have used sixty characteristic curves, the initial conditions for the i-th characteristic being:

$$x_0^i = \cos\theta_0^i\,,\quad y_0^i = \sin\theta_0^i\,,\quad \theta_0^i = 2\pi/i\,,\quad for\ i = 1\ldots 60\,, \tag{37}$$

$$\begin{aligned}\widetilde{\sigma}_0^i &= \ln(1-0.5\exp(-1000(1.29-\cos\theta_0^i-0.4\sin\theta_0^i)^2)+\exp(-1500(1.1+0.2\cos\theta_0^i-0.6\sin\theta_0^i)^2)\\ &- 0.5\exp(-1000(1.29+\cos\theta_0^i+0.4\sin\theta_0)^2))\,.\end{aligned}$$

We present in Figures 3 and 4 the results obtained for two current patterns with $m = 1$ and 2 for data with 2% random errors. The reconstructed conductivity obtained lies at a distance $\|\sigma - \sigma_{exact}\|_{L^2} = 0.07\|\sigma_{exact}\|_{L^2}$ for $m = 1$ and at $\|\sigma - \sigma_{exact}\|_{L^2} = 0.09\|\sigma_{exact}\|_{L^2}$ for $m = 2$ from the true function. We see that in the both cases the L^2 norm of the difference between the target and the model has been reduced significantly. It is interesting to note that these results are quite similar and that it appears that little can be gained by using more patterns. In our method the interest of using extra current patterns is in the calculation of a good model function Y_{mod}.

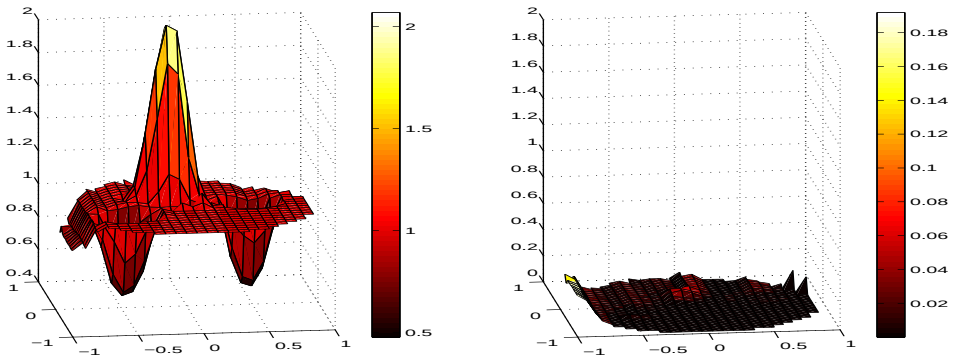

(a) (b)

Figure 3: The reconstructed conductivity using $\sin(\theta)$ for data with random 2% errors
(a) - the reconstructed conductivity $\sigma(x, y)$; (b) - the absolute errors $\mid \sigma(x, y) - \sigma_{exact}(x, y) \mid$

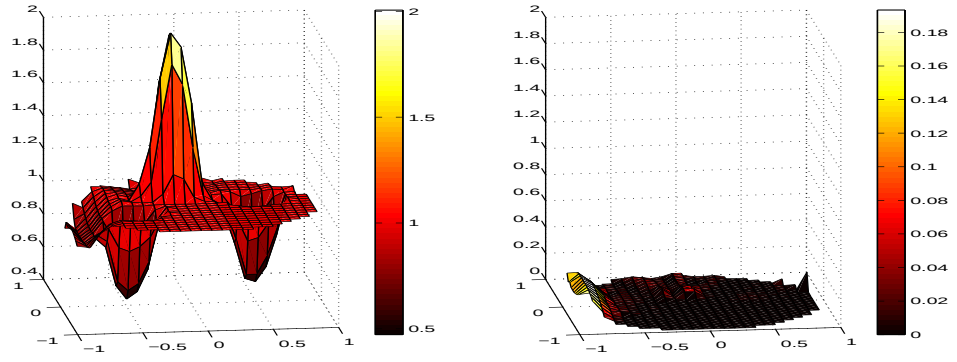

(a) (b)

Figure 4: The reconstructed conductivity using $\sin(2\theta)$ for data with random 2% errors
(a) - the reconstructed conductivity $\sigma(x, y)$; (b) - the absolute errors $\mid \sigma(x, y) - \sigma_{exact}(x, y) \mid$

8.The notch of the ϵ_0 graph

We finally discuss an example, in which the position and/or orientation of the target function is described by a small number of parameters. Such a situation occurs for example in land mine detection, where the type of objects we are seeking (i.e. the model function) is quite well known and it is their location which we wish to determine. This example takes into consideration the action of some group of operators acting on the model function. In practice we shall encounter mainly the action of the Euclidean group of rotation and translations.

An interesting feature of this kind of problem is that we are no longer in the ball regularization geometry where one often encounters the situation in which the final solution does not represent an improvement with respect to the model function. This arises in simple ball regularization since the fact that both the target function Y_{exact} and the solution Y_{reg} lie on the surface of an infinite dimensional sphere of radius δ centered at Y_{mod} does not necessarily imply that $\|Y_{reg} - Y_{exact}\|_{L^2} < \|Y_{mod} - Y_{exact}\|_{L^2} = \delta$ (see Figure 5). In two dimensions we can see that the probability that this is true is only $1/3$ as Y_{exact} needs to lie on the 120^0 bold face arc around Y_{reg}, while, in the infinite dimensional case this probability reduces to $1/4$. This is certainly disappointing, but this situation will no longer hold if Y_{mod} depends on some unknown parameter(s) α so that the geometry of the regularization set is no longer spherical. We then try to find the optimal value α_0 of the parameter α (see Section 5) by plotting the graph of $\epsilon_0(\alpha)$ defined in equation (24).

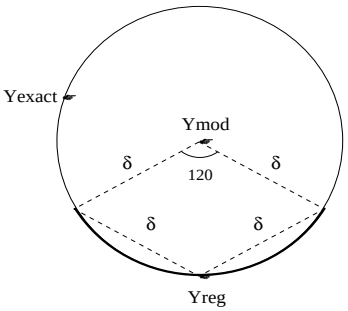

Figure 5: In two dimensions the probability that $\|Y_{reg} - Y_{exact}\|_{L^2} < \|Y_{mod} - Y_{exact}\|_{L^2} = \delta$ is only $1/3$ as Y_{exact} needs to lie on the 120^0 bold face arc around Y_{reg}.

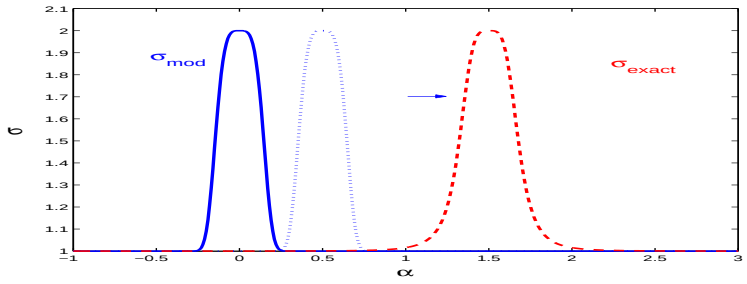

(a) The translation of σ_{mod} towards σ_{exact} for different values α.

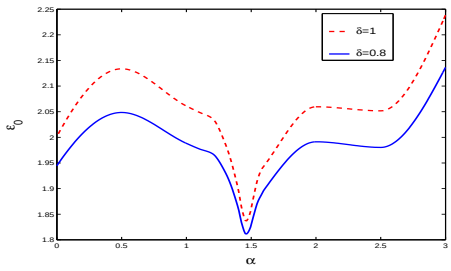

(b) The notch of the graph $\epsilon_0(\alpha)$ for two different $\delta = \|Y_{reg} - Y_{exact}\|_{L^2}$

Figure 6: The notch method.

As an example, we consider the problem of the lower half plane in which the conductivity depends on a parameter α. The target conductivity has a maximum on the $y = -1$ axis at a point corresponding to $\alpha_0 = 1.5$. To illustrate how this procedure works we consider only the translations of the model function along the line $y = -1$, for $\alpha \in [0, 3]$ (see Figure 6 (a)). We represent the target conductivity distribution by

$$\sigma_{exact} = 1 + \frac{a}{((x - \alpha_0)^2 + (y + 1)^2)^2 + b}$$

and we choose the model function of the form

$$\sigma_{model} = 1 + \exp(-c((x - \alpha)^2 + (y + 1)^2)^2)\,.$$

We chose $a = b = 0.001$ and $c = 1500$.

By means of a conformal mapping we transfer the problem onto the unit disk and proceed as described earlier for different values of α. Since this is only an illustrating example, in the regularization functional (24) we used the unweighted L^2 norm for the unit disk which means that for the initial half plane we used the norm induced by the Jacobian of the inverse mapping. This norm has compactifying properties but it depends on the conformal mapping. Even in this rough treatement we see that this method is quite sensitive since the notch in the graph of $\epsilon_0(\alpha)$ is quite narrow (see Figure 6 (b)). The position of this minimum of the graph $\epsilon_0(\alpha)$ gives the location of the object we look for and represents the best

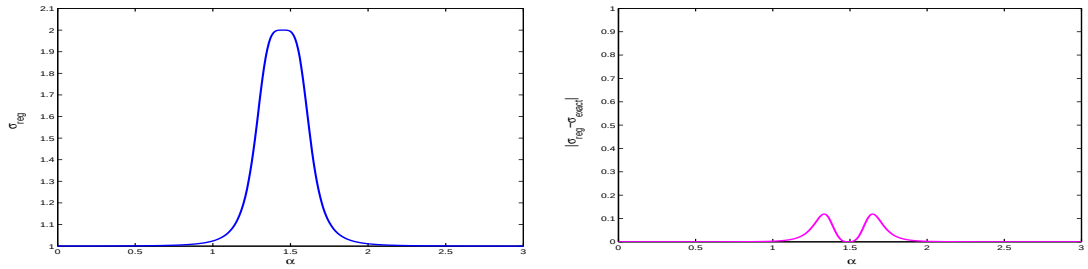

(a) The regularized conductivity σ_{reg}.

(b) The absolute errors $|\sigma_{reg} - \sigma_{exact}|$.

Figure 7: The reconstructed conductivity using the notch method.

value of α to use in our model. The conductivity distribution reconstructed using this method is shown in Figure 7.

9. Conclusion

We have presented a reconstruction algorithm based on a Tikhonov regularization of a formulation of the inverse conductivity problem in terms of integral equations. The method uses prior information in the form of a model conductivity distribution. Our numerical experiments have shown the importance of this model and that multiple data appear to have little effect on our results. We have suggested ways in which more data measurements may be used to improve the model but numerical results suggest that our technique may prove to be useful in situations in which complex data collection is difficult but we have a good qualitative information on the conductivity distribution .

Acknowledgements: We would like to thank Guy Auberson, Gérard Mennessier and Valentin Poenaru for useful conversations concerning this work, and The Leverhulme Trust for providing financial support.

References

[1] A. P. Calderón, *Seminar on Numerical Analysis and its Applications to Continuum Physics*, Soc. Brasileira de Matemàtica, Rio de Janeiro, 65-73, (1980).

[2] R. Kohn and M. Vogelius. *Determining conductivity by boundary measurements II. Interior results.* Comm. Pure Appl. Math., **38**, 643-667, (1985).

[3] J. Sylvester and G. Uhlmann. *Inverse boundary value problems at the boundary - Continuous dependence.* Comm. Pure Appl. Math, **41**, 197-221, (1988).

[4] A. I. Nachman. *Global uniqueness for a two-dimensional inverse boundary problem.* Ann. Math., **142**, 71-96, (1995).

[5] D.J. Cedio-Fenygya, S. Moscow and M.S. Vogelius, *Identification of conductivity imperfections of small diameter by boundary measuremens. Continuous dependence and computational reconstruction.* Inverse Problems **14**, 553-594, (1998).

[6] M. Brűhl and M. Hanke, *Numerical implementation of two noniterative methods for locating inclusions by impedance tomography.* Inverse Problems **16**, 1029-1042, (2000).

[7] M. Brűhl, M. Hanke and M. Vogelius, *A direct impedance tomography algorithm for locating small inhomogenities*, Numer. Math. **93**, 635-54, (2003).

[8] S. Siltanen, J. Mueller and D. Isaacson, *An implementation of the reconstruction algorithm of A Nachman for the 2D inverse conductivity problem*, Inverse Problems **16**, 681-699, (2000).

[9] S. Ciulli, M. Pidcock, T.D. Spearman and A. Stroian, *Image reconstruction in Electrical Impedance Tomography using an integral equation of the Lippmann-Schwinger type*, Phys Letters A **271**, 377-384, (2000).

[10] S. Ciulli, M. Pidcock and C. Sebu,*On the inverse conductivity problem in the half space.*, Z. Angew. Math. Mech. 83 **11**, 755-765, (2003).

[11] W. W-G. Yeh, *Review of parameter identification procedures in ground water hydrology: The inverse problem*, Water Res. Res. **22**, 95-108, (1986).

[12] G. R. Richter, *An inverse problem for the steady state diffusion equation*, SIAM J. Appl. Math. **41**, 210-221, (1981).

[13] G. Alessandrini, *An identification problem for an elliptic equation in two variables*, Ann. Math. Pura Appl. **145**, 265-296, (1986).

[14] G. Chavent and K. Kunisch, *New results on the non-linearity and the sensitivity of the estimation of the diffusion coefficient in a 2D elliptic equation*, Inverse Problems in Engineering: Theory and Practice (ed. K. Woodbury), ASME, 91-96, (1999).

[15] A. Farcas, L. Elliot, D. B. Ingham and D. Lesnic, *A DRM for solving the inverse problem of steady groundwater flow*, Proceedings of the Fourth UK Conference on Boundary Integral Methods (ed. S. Amini), Salford University, 87-96, (2003).

[16] G. de Rham, *Variétes Différentieles – Formes, courants, formes harmoniques*, Hermann, (1973).

[17] John W. Milnor, *Morse Theory*, Princeton University Press, (1963).

[18] R. Courant and D. Hilbert, *Methods of Mathematical Physics*, Vol. I. John Wiley & Sons, New York, (1989).

[19] H. W. Engl, M. Hanke and A. Neubauer, *Regularization of Inverse Problems*. Kluwer Academic Publishers, (2000).

[20] S. Ciulli, C. Pomponiu, I. Sabba-Stefanescu, *Analytic Extrapolation Techniques and Stability Problems in Dispersion Relations Theory*, Physics Reports, **17C**, 133-224, (1975).

[21] S. Ciulli, M.K. Pidcock and C. Sebu, *An analytical solution for the inverse conductivity problem*, Proceeding of The First Romanian Conference of Theoretical Physics (Sept 2002), Rom. Journ. Phys. **48**, 50-61, (2003).

[22] Michael Reeds and Barry Simon, *Methods of Modern Mathematical Physics I: Functional Analysis*, 2nd ed.,Academic Press, San Diego, CA (1980).

[23] Kosaku Yosida, *Functional Analysis*, Springer-Verlag, 120-125, (1965).

[24] M. Ciulli, S. Ciulli and T. D. Spearman, *Weak-star compactness and its relevance to analyticity problems*, Rigorous Methods in Particle Physics, Springer Tracts in Modern Physics, **119**, 102-125, (1990).

[25] C. Sebu, *Inverse Problems in Classical and Quantum Physics*, PhD thesis, Univ. Montp. II, (2004).

[26] H. Engels, *Numerical quadrature and cubatures*. Academic Press, London, (1980).

[27] P.C. Hansen, *Regularization Tools: A Matlab Package for Analysis and Solution of Discrete Ill-Posed Problems*.